Hindawi
Shock and Vibration
Volume 2022, Article ID 4334398, 12 pages
https://doi.org/10.1155/2022/4334398

Research Article

Vibration Transmission Characteristics and Measuring Points Analysis of Bearing Housing System

Wenbing Tu,[1] Jinwen Yang,[1] Ya Luo,[1,2] Lianbao Jiang,[3] Jin Xu,[4] and Wennian Yu[3]

[1]*School of Mechanotronics and Vehicle Engineering, East China Jiaotong University, Nanchang 330013, China*
[2]*State Key Laboratory of Performance Monitoring and Protecting of Rail Transit Infrastructure, East China Jiaotong University, Nanchang 330013, China*
[3]*College of Mechanical and Vehicle Engineering, Chongqing University, Chongqing 400044, China*
[4]*China North Vehicle Research Institute, Beijing 100081, China*

Correspondence should be addressed to Wennian Yu; wennian.yu@cqu.edu.cn

Received 2 December 2021; Accepted 7 February 2022; Published 27 February 2022

Academic Editor: Liu Jing

The vibration transmission characteristics of the bearing housing system are crucial for the system fault diagnosis based on vibration signals collected at various measuring points. To study its vibration transmission characteristics, a dynamic model of the rolling bearing housing system based on the elastic interface is established. The interference fit between the bearing outer ring and the bearing housing is modelled by contact pairs. The proposed model is verified by the experimental results, which demonstrate that the interference fit can be better simulated by contact pairs. Based on the comparisons between the vibration signals obtained from the defect point and the measuring points on the bearing surface, the transmission mechanism of the defect excitation and the generation mechanism of the bearing housing structural vibration are clarified. The change law of defect excitation through an interface and the effects of bearing operational conditions (load and speed) on the vibration signals of measuring points are summarized. The results show that the optimal measuring point on the bearing housing surface is the location that is closest to the defect when the bearing housing system is working under light loads or high speeds. However, when under low speeds, the preferred measuring points are the positions where the rigidity of the bearing housing structure is weak. The analysis results provide a theoretical basis for the sensor arrangement and improvement of fault diagnosis accuracy under different operating conditions.

1. Introduction

Rolling bearings are one of the most eventful components in machinery and equipment. The acquisition and analysis of vibration signals are important to monitor their internal operating status [1, 2]. To improve the accuracy of bearing fault diagnosis, it is important to study the vibration transmission mechanism caused by the bearing defect excitations. There has been plentiful research on it in the literature carried out by different scholars [3–5]. Singh et al. [6, 7] analyzed the dynamic contact force and vibration mechanism between the rolling elements and the outer race with the bearing spalling defect. Ahmadi et al. [8] included the mass of the rolling element in their model and studied the relationship between the vibration response and the internal force of the defect bearing. Patel et al. [9] studied the nonlinear vibration response of the bearing with a local defect on the race and investigated the contact relationship between the rolling element and fault. Liu et al. [10, 11] proposed a dynamic model of the planet roller bearing considering the cage crack to detect the initial cage crack failure in the planet roller bearing.

Although scholars have achieved a lot of progress in the study of the vibration mechanism of bearing with defects, the accuracy of fault diagnosis is still limited due to the shortcomings of signal acquisition methods. Traditional methods generally install the sensors on the outer surface of the bearing housing to collect the vibration signals of the

bearing. However, the collected signals cannot faithfully reflect the characteristics of bearing internal excitation due to the inevitable attenuation when the defect excitation transmits through contact interfaces between the bearing outer race and the bearing housing. Moreover, when the transmission route is long, it is difficult to accurately diagnose the fault status inside the bearing. Shao et al. [12] used the experimental methods to study the vibration transmission characteristics of rolling bearings and proposed the energy retention factor to describe the dissipation of vibration energy through multiple interfaces. However, since it is rather challenging to measure the bearing internal excitation, the transmission mechanism between the bearing internal excitation and the outer vibration response collected by the sensors cannot be experimentally investigated. Alian et al. [13] proposed to use the fiber-optic sensors to measure the strain of the rolling bearing for defect diagnosis, which can be mounted inside the bearing. However, most of the current signal processing algorithms are based on the vibration signal, and there are very few for the strain signal.

Therefore, it is necessary to investigate the vibration transmission mechanism along the interface between the outer race and housing for effective fault detection and diagnosis. White [14] took the flexibility of the housing into account and proposed a two-degree-of-freedom dynamic model to study the vibration transmission characteristics of the rolling element bearing. Lim and Singh [15] considered the coupling effect between the bearing and the housing and developed a five-degree-of-freedom dynamic model to investigate the vibration transmission through rolling element bearings. Gao et al. [16] assumed a rigid connection between the outer race and the housing and established a vibration model of the cylindrical roller bearing system, from which the influence of bearing housing deformation on the vibration characteristics was studied. Kraus et al. [17] and Fleming [18] included the flexibility of the bearing housing in their dynamic model and discussed the vibration transmission characteristics of a rotor-bearing housing system. Although the above work focused on the vibration transmission characteristics of the bearing-bearing system, a rigid connection is usually assumed between the outer race and the housing in their models, and the elasticity of the interfaces between them is ignored. These make it impossible to accurately describe the discrepancies between the vibration of the outer race and vibration of the housing caused by the bearing internal excitation.

To address this issue, Liu et al. [19–21] proposed a dynamic model to study the vibration transmission of a shaft-bearing housing system with a localized fault. In this model, elastic interfaces were considered, and the vibration transmission characteristics along multiple interfaces caused by the rolling bearing internal impact excitation were investigated. Xiao et al. [22] established an 8-DOF dynamic model for a gear-shaft-bearing housing system with elastic interfaces and studied the vibration transmission characteristics and energy dissipation characteristics of pulse excitation generated by gear fault passing through multiple interfaces. Although the above models considered the elastic interface relationship between the outer race and the housing, the elastic deformation of the bearing seat is ignored. In addition, the excessive rigidity of the structure will increase the amplitude of acceleration, which is usually neglected. In addition, existing dynamic models cannot reflect the actual interference fit relationship between interfaces. The fit clearance between the rolling bearing outer race and the housing plays a significant role in the vibration response, as argued by Chen and Qu [23]. Thus, the simulation signals obtained by the abovementioned models do not faithfully reflect the practical situations.

With the development of computer science, the finite element method provides an effective way to simulate the actual mechanical properties of the materials and the interference assembly relationship between the bearing and the housing with the elastic interfaces. Wang et al. [24] considered the elastic deformation of the materials and simulated the interference connection between the bearing and the housing using the common nodes. A finite element model for the bearing housing system was established. The transmission characteristics of the vibration signal between the bearing outer race and the housing were investigated to find the optimal position and direction for the measuring points on the housing. The bearing defect excitation was simulated by a periodic impact load in the model, which is quite different from the actual defect excitation. Cao et al. [25] and Xiang et al. [26] regarded the bearing outer race and the housing as a whole to simulate the interference connection of the interfaces. The vibration transmission of the gear-shaft-bearing housing system was investigated, and a structure optimization strategy was proposed to reduce the transmission error. However, the vibration transmission characteristics between the bearing and the housing were not specifically analyzed.

In summary, there are deficiencies in the existing analytical models as they cannot model the elastic deformation of the housing and the connection relationship of interfaces. Although the finite element model can consider the effect of the practical interference connection between the bearing and the housing on the vibration transmission characteristics, it generally uses the sharing nodes to simulate the interference fit of the interfaces, which cannot reflect the actual contact situation. Therefore, a rolling bearing housing system dynamic model still lacks that comprehensively considers the elastic interface, interference assembly relationship, and fault morphology. In addition, the difference between the vibration signals inside the bearing and outside the housing caused by the defect excitation and the distribution law of the optimal measuring points under different speed and load conditions are not sufficiently understood. In this article, a dynamic model of a rolling bearing housing system based on an interference interface and an elastic interface is established. The bearing defect is simplified to a rectangular shape. The interference assembly relationship between the bearing and the housing is modelled by sharing nodes and a contact pair between interfaces. The proposed model is verified by the experimental results, which overcomes the shortcomings of the current models that cannot accurately describe the difference of vibration characteristics between the outer

race and the housing. Based on the analysis of the vibration signals obtained from the defect point and various measuring points on the housing surface, the transmission mechanism of the defect excitation and the generation mechanism of the bearing housing structural vibration are clarified. The effects of load and speed on the defect excitation transmission and structural vibration are studied, which can provide a theoretical basis for optimal sensor placement under different operating conditions and improve the accuracy of bearing fault diagnosis.

2. Dynamic Model

2.1. Problem Description. In practice, the health condition of the rolling bearing during operation is generally monitored by collecting vibration signals through accelerometers that are mounted on the bearing housing (which is referred to as measuring points in the remainder of this article). Once a defect is generated inside the bearing (either inner race or outer race, balls, etc.), there will be significant periodic impacts in the vibration signals. These impacts are originated from collisions between components with defects and transmit from the interior bearing to the exterior bearing housing. Due to the variations of the vibration transmission path from the defect point to the measuring points, the signals collected at different measuring points caused by the same defect excitation are different, as shown in Figure 1(a). The vibration signal is weakened to varying degrees when it transmits from the excitation source to the surroundings. In addition, because the thickness of the bearing housing is uneven in the circumferential direction, the structural rigidity in each direction is different, and the structural vibration generated at different positions is also different, as shown in Figure 1(b). Therefore, the vibration signals collected by the sensors at different positions on the surface of the bearing housing will be greatly different due to the uncertainty of the defect excitation and the structure vibration.

To study the relationship of the vibration signals between the defect point and the measuring points at different positions on the bearing housing, it is necessary to investigate how the defect excitation is transmitted to the bearing housing and how the structural vibration is generated in the bearing housing. The optimal sensor installation position to obtain the most accurate bearing defect signal can thus be found. It is also noted that both the load and speed affect the defect excitation significantly. Therefore, the effects of the load and speed on the transmission of defect excitation and structural vibration are further studied, which can provide theoretical guidance for the arrangement of sensors and improve the bearing fault diagnosis under different operating conditions.

2.2. Establishment of Model. This study takes the cylindrical roller bearing NU306 as the research object. Its main geometric parameters are given in Table 1. The explicit dynamics software package, LS-DYNA, is used for finite element simulation.

Since the cross-section of the cylindrical roller bearing along its axis is the same and only the radial load is supported by the bearing, a two-dimensional model is built for the bearing to improve the computation efficiency. The 2D plane strain element SHELL163 is used as the solid structure for the bearing and the bearing housing in the model. Due to the nonlinearity of the internal contact of the bearing, the triangular mesh should be minimized to ensure the accuracy of the simulation results. Therefore, the bearing housing, the rings, the cage, and the rolling elements are all meshed by quadrangle elements. To obtain accurate dynamic responses, it is generally recommended that the wavelength of the transmission signal should be 20 times larger than the grid size of the structure for wave propagation studies. Considering the outer race as a thin plate, the speed of bending waves C_b is given by [6]:

$$C_b = \sqrt{\omega}\left[\frac{ET^2}{12\,(1-\nu^2)\rho}\right]^{1/4}, \tag{1}$$

where E, ρ, υ, T, and ω are the modulus of elasticity, density, Poisson's ratio, thickness, and angular frequency, respectively. Substituting their values into the above formula, and assuming the frequency is 40 kHz and the thickness of the thin plate is 19 mm, the bending wave velocity is about 2007.73 m/s, and the corresponding wavelength is about 0.0675 m. Thus, the maximum grid size should be smaller than 3.375 mm. To ensure the continuous contact between the rolling elements and the outer race and to minimize the vibration noise caused by the regular polygon effect of the grid, models with grid sizes of 1 mm, 0.5 mm, and 0.25 mm were established for trial calculation, respectively. By comparing the contact force curves between the rolling elements and the races, it was found that the contact force curve is discontinuous when the grid size is large, but it becomes smooth when the grid size is reduced to a certain value. Therefore, in this article, the mesh size of the components with contact behavior (including the races, rolling elements, and cage) is set to 0.25 mm, and the mesh size of the bearing housing without contact behavior is set to 1 mm. The defect studied in this article is located on the outer race. Thus, the mesh in the contacting area of the outer race is refined. There are about 77894 nodes and 75140 elements, which are shown in Figure 2. This article is concerned with the vibrations generated due to a local line spall in the outer raceway, and the defect is simplified into a fully penetrating rectangular recess. The defect is located directly at the bottom of the bearing, whose width and depth are both 1 mm.

The elastic materials are used for the bearing components to consider the influence of the elastic interface between the outer race and the bearing housing. The rolling elements and the races are modelled by the steel GCr15, whose material properties are as follows: density $\rho_1 = 7830\,\mathrm{kg\,m^{-3}}$, modulus of elasticity $E_1 = 206$ GPa, and Poisson's ratio $\nu_1 = 0.3$. The cage is modelled by the brass, whose material properties are as follows: density $\rho_2 = 8500\,\mathrm{kg\,m^{-3}}$, modulus of elasticity $E_2 = 105$ GPa, and Poisson's ratio $\nu_2 = 0.324$. The boundary conditions for the FE model are given as follows:

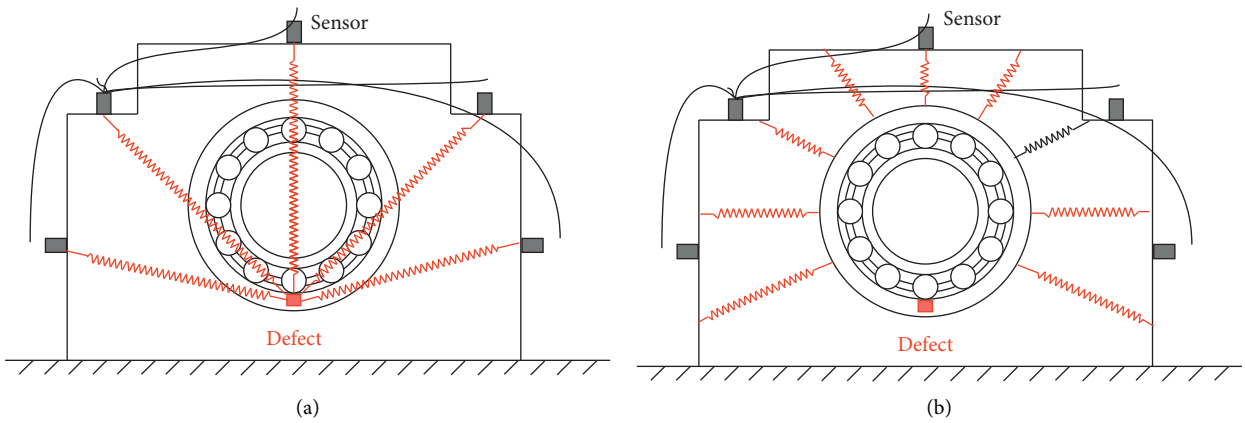

Figure 1: Schematic diagram of defect vibration transmission of the bearing housing system: (a) Defect excitation and (b) structure vibration.

Table 1: Geometric parameters of the cylindrical roller bearing NU306 [4].

Geometric parameter	Value
Roller diameter (D_r, mm)	11
Bearing pitch circle diameter (D_m, mm)	51.5
Bearing inner diameter (D_i, mm)	30
Bearing outer diameter (D_o, mm)	72
Thickness of outer race (T, mm)	19
Contact angle (α, °)	0
Roller number (Z)	12
Radial clearance between roller and races (ε_1, mm)	0.01
Cage pocket clearance (ε_2, mm)	0.08

(1) Three different radial loads, i.e., 3000 N, 2000 N, and 1000 N, are applied to the inner surface of the inner race in the negative direction of the Y-axis.

(2) Four different speeds, i.e., 700 rpm, 1400 rpm, 2100 rpm, and 2800 rpm, are applied to the inner race in the counterclockwise direction.

(3) All degrees of freedom at the bottom of the bearing housing are constrained, as shown in Figure 2.

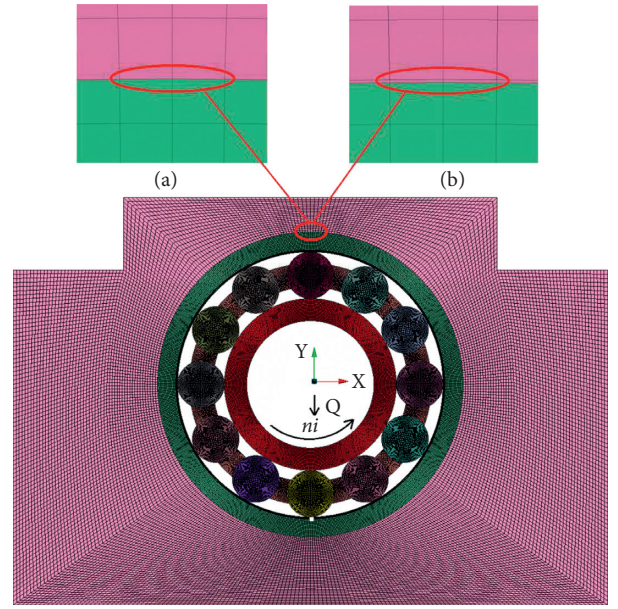

Figure 2: Two-dimensional finite element model of the bearing housing system: (a) common node model and (b) contact pair model.

The basic surface-to-surface contact type in 2D contact is used to simulate the contact situation during bearing operation. A penalty method is used to formulate the contact between two contact components. In this contact algorithm, the slave surface is checked for penetration through the master surface. As shown in Figure 3, in order to determine the positional relationship between two contact points $x^1(\xi^1, t)$ and $x^2(\xi^2, t)$, a gap parameter g_n is defined by

$$g_n = \min \lambda \left\| x^1\left(\xi^1, t\right) - x^2\left(\xi^2, t\right) \right\|, \tag{2}$$

where λ is a distance parameter, which is given by

$$\lambda = \begin{cases} 1\left(x^2 - x^1\right)\eta^1 \le 0 \\ -1\left(x^2 - x^1\right)\eta^1 > 0 \end{cases}, \tag{3}$$

where η^1 describes the normal vector for body #1, and t is the time. In this algorithm, g_n describes the position relationship between the two contact points, with $g_n > 0, = 0$, and < 0 representing the two points as in penetration, in contact, and out of contact, respectively. The normal contact force F_c is given by

$$F_c = -\frac{g_n \alpha_f E_b S_b}{\max(\text{shell\_diagonal})} \tag{4}$$

where α_f is a scaling coefficient, whose value is usually considered as 1; E_b is the bulk modulus, which is a function of Poisson's ratio and elastic modulus of the material; S_b is the area of elements in contact.

The inner race, the outer race, and the cage are defined as the master segments, and the rolling elements are defined as the slave segments. Moreover, 36 contact pairs are established for the 12 rolling elements, and each has three contact pairs with the inner race, the outer race, and the cage,

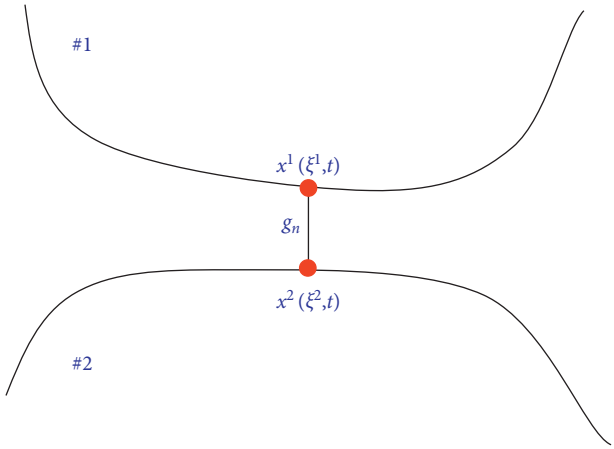

Figure 3: Contact relationship between the contact points.

respectively. The static friction factor is set to 0.01 and the dynamic friction factor is set to 0.005.

In practice, the interference fit is usually used between the outer race and the bearing housing. The interaction and contact deformation between the two interfaces will certainly affect the vibration transmission mechanism due to the bearing defect excitation. Thus, the influence of the elastic interfaces between the bearing outer ring and the housing must be considered. In previous work that uses the finite element model to simulate the interference connection between the outer race and the bearing housing, sharing node model was generally established for the outer race and the bearing housing [24, 27, 28] (i.e., mode #1), which means that the outer race and the bearing housing are considered as a whole body and there is no contact relationship between them, as shown in Figure 2(a). In this work, we use another model (i.e., mode #2) to simulate the interference connection. A contact pair between the outer race and the bearing housing is established, which sets a contact relationship between the interfaces and allows a small amount of penetration between them. To prevent the outer race from rotating, the static friction factor between the outer race and the bearing seat [7] is set to be 0.1, as shown in Figure 2(b).

3. Results and Discussion

3.1. Experimental Verification. A rolling bearing (NU306) experimental system was set up, as shown in Figure 4. To ensure the consistency between the test conditions and the FE modelling, a defect of size 1 mm × 1 mm (width × depth) was implemented on the outer race of the bearing, and an interference fit was achieved when mounting the bearing outer race on the bearing housing. A radial load of 3000 N was applied on the bearing housing by screwing a thrust device JL1086 and the load was instantaneously measured via a pressure strain gauge. The bearing inner race was driven by a servo motor at a speed of 2100 rpm. The accelerometers were placed on the top surface and side surface of the bearing housing, respectively. After the experimental bearing was running stably, the time-domain acceleration signals collected by the sensors were transmitted to a computer for preliminary analysis and data storage via a signal acquisition card NI USB-4431. The measured acceleration signals are directly compared with the simulation results based on the abovementioned two FE models, as shown in Figure 5. Figure 6 shows the corresponding envelope spectrums of the signals in Figure 5.

From Figure 5, it can be found that the periodic impacts due to the bearing defect are obvious in the simulated signal based on mode #2, which shows a good agreement with the experimental results in terms of the impact shape and amplitude, no matter on the top surface or the side surface of the bearing housing. However, they are very trivial in the simulated signal based on mode #1. From Figure 6, it can be found that the fault characteristic frequency of the simulated signal is approximate to that of the experimental signal. The slight relative error may be caused by the fluctuation of the rotation speed of the cage. This result proves the validity of the proposed model (model #2). In addition, compared with the spectrum based on mode #1, the outer race defect frequency and its harmonics can be more clearly identified in the spectrums based on mode #2 and experimental results. These demonstrate the accuracy of the proposed model in simulating the vibration transmission between interfaces of the bearing outer race and bearing house against the previous model (model #1). In fact, in mode #1, the outer race and the bearing housing are modelled as a whole, and the interaction force between the interfaces that will affect the vibration transmission is ignored. The proposed model #2 can accurately capture the interactions and thus yield consistent results with the experiment. Therefore, it is necessary and reasonable to simulate the interference fit using contact pairs in the finite element model, which can more closely simulate the real operation of the bearing. In the following sections, we will study the vibration transmission characteristics at several measuring points based on the proposed FE model.

3.2. Vibration Transmission Characteristics of Bearing Housing System and Selection of Measuring Points. In this section, the vibration transmission characteristics of the bearing housing system at various measuring points will be studied based on the proposed FE model. Since the bearing housing has a symmetrical structure, we consider eight evenly distributed measuring points (marked as points #1, #2, . . ., #8) on half of the bearing housing surface, as shown in Figure 7. The acceleration signal of measuring point #0 is considered as the defect excitation as it is directly located at the defect point. The root mean square (RMS) of the acceleration signals collected at the above points is calculated. The vibration transmission ratio can be expressed by the RMS value at each measurement point with respect to the RMS value of defect excitation. The transmission ratios in the X-direction and Y-direction are shown in Table 2.

In the actual signal acquisition process, the sensors at the measuring points #1, #2, and #4 are generally used to obtain the acceleration signals in the Y-direction, and the measuring points #3, #5, #6, #7, and #8 are used to obtain the acceleration signals in the X-direction. According to Table 2,

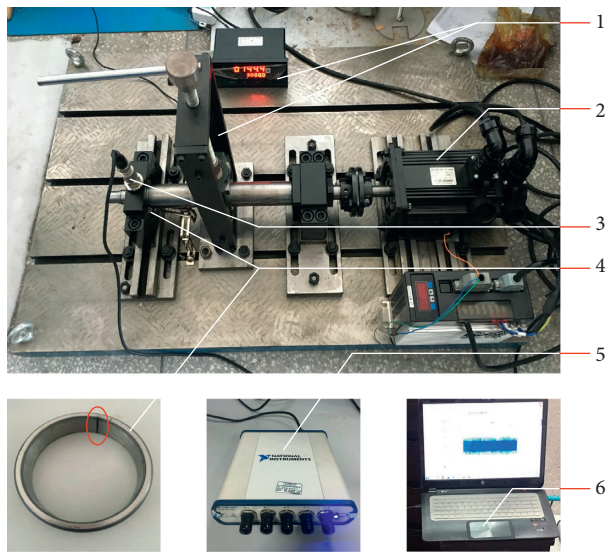

Figure 4: Rolling bearing experimental system (1, radial loading device; 2, servomotor; 3, accelerometer; 4, defect on the bearing outer race; 5, signal acquisition card; 6, computer).

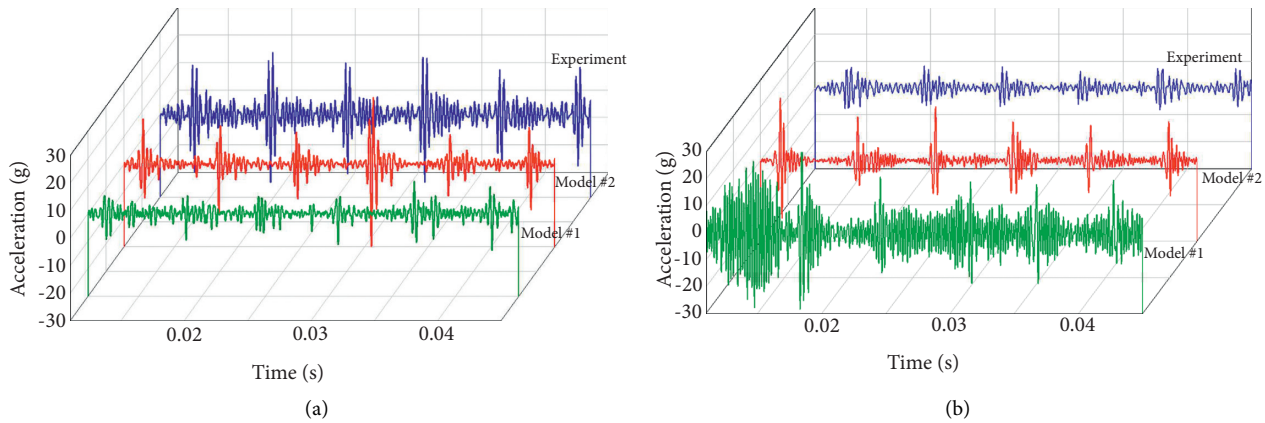

Figure 5: Time-domain acceleration signals from (a) the top surface of the bearing housing and (b) the side surface of the bearing housing.

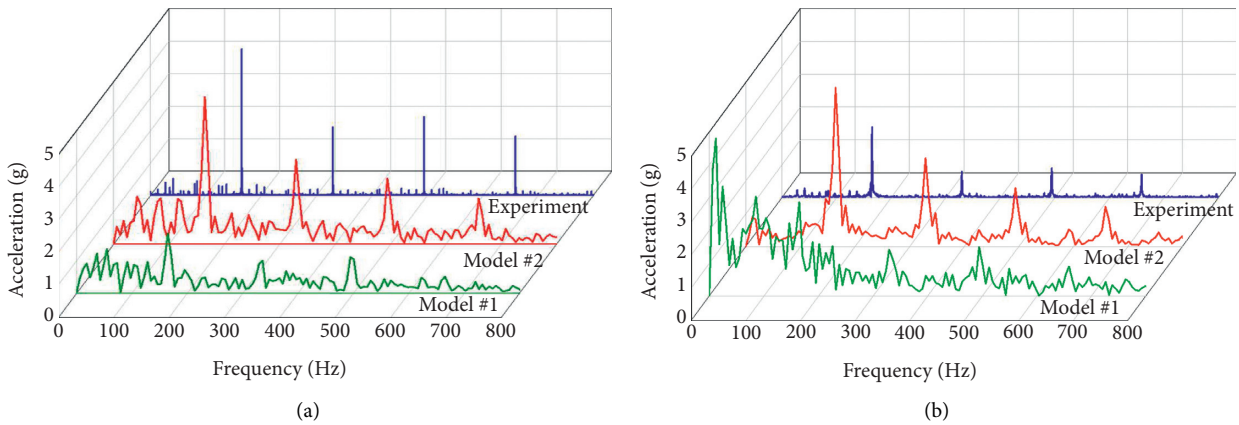

Figure 6: Envelope spectrum of the vibration signals from (a) the top surface of the bearing housing and (b) the side surface of the bearing housing.

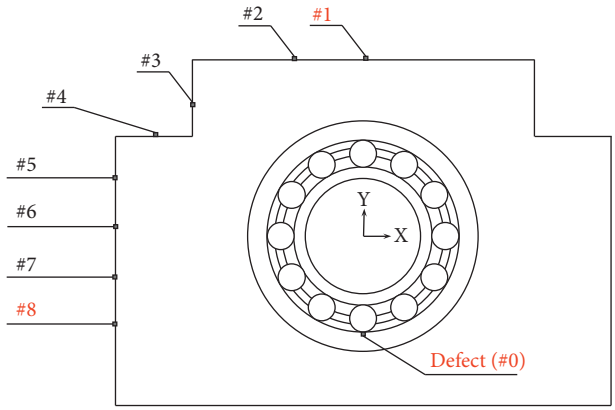

Figure 7: The location of the measuring points.

Table 2: The vibration mission ratio at different measuring points in the X- and Y-directions.

Measuring point	Ratio (X-direction)	Ratio (Y-direction)
Point #1	24.89	47.38
Point #2	25.63	35.22
Point #3	24.34	40.87
Point #4	36.92	35.30
Point #5	25.84	49.08
Point #6	27.64	30.08
Point #7	27.03	34.02
Point #8	31.23	36.85

it can be found that point #1 has the largest transmission ratio (47.38%) among the measuring points for acquiring the Y-direction signal, and point #8 has the largest transmission ratio (31.23%) among the measuring points for acquiring the X-direction signal. These indicate that the vibration energies at these two points are the largest among them all. The reason can be possibly explained by the deformation cloud diagram inside the bearing housing while a rolling element is passing through the defect, as shown in Figure 8. It should be noted that the larger transmission ratio of point #4 and point #5 in the nonvibration-measurement direction is possibly due to the special structure of the bearing housing. The elastic deformation of the bearing housing is considered and point #4 and point #5 are located in the place where the shape of the bearing housing changes sharply. The sharp corner is prone to stress concentration, which causes an abnormal increase in local vibration. Although the transmission ratio of point #4 in the X-direction is larger than that of point #8, point #4 is mainly used to obtain the vibration in the Y-direction, and the vibration transmission ratio of point #8 in the X-direction is still the greatest. Similarly, although the transmission ratio of point #5 in the Y-direction is larger than that of point #1, point #5 is mainly used to obtain the vibration in the X-direction, and the vibration transmission rate of point #1 is still the largest in the Y-direction.

According to Figure 8, as the rolling element passes through the defect, the deformation of the bearing housing gradually decreases from the contact area between the outer race and the bearing housing to the surroundings. It indicates that the vibration of the outer race caused by the defect will be transmitted from the contact area to the surface of the bearing housing. Since point #8 is the closest point to the bearing surface (except the bottom area of housing which is fixed), the vibration at this point is relatively large. In addition, it can be noticed that the deformation cloud near point #1 is always the largest when the rolling element is passing through the defect. Figure 9 shows the profile of bearing housing without and with the deformation (i.e., Figure 8(c)) with an enlarged scale of 200.

Due to the uneven thickness of the bearing housing around the bearing outer race, the structural stiffness around the outer race is different, and the magnitude of deformation is also different. Since the thickness of the housing upper part is the smallest, its structural rigidity is the smallest. In addition, the inner diameter of the bearing housing in the vertical direction is elongated due to the influence of load and defect. Thus, the deformation at the housing upper part near point #1 is the largest.

In conclusion, points #1 and #8 can better reflect the characteristics of the vibration signal due to the defect excitation. This is because that point #8 is the closest point to the defect, and the structural stiffness near point #1 is relatively small. Therefore, the best vibration-measurement point on the surface of the bearing housing should be at the location with a small structural stiffness or closest to the fault.

3.3. Analysis of Vibration Signals at Measurement Points under Different Loads. To further investigate the influence of load on the vibration attenuation from the interior defect point to the exterior measuring points, the vibration signals at the defect point and the measuring points are compared. The vibration signals in the Y-direction (i.e., the vertical direction) at the measuring point #1 and the defect point (i.e., point #0 as shown in Figure 7) under radial loads of 3000 N, 2000 N, and 1000 N are shown in Figure 10.

It can be seen from Figure 10 that the larger the load, the greater the amplitude of the impulses in the time-domain vibration signals for both points #0 and #1. This demonstrates that the defect characteristics become clearer as the load increases. Compared to point #0, the impact component in the vibration signals at point #1 is weaker, and the noise and other components are more obvious. This is due to the influence of energy dissipation and structural vibration when the vibration signal propagates from the defect source to the measurement point. In the case of a large load, the defect impact in the vibration signals at point #1 is obvious. As the load decreases, the impact components are submerged by noise. The defect characteristics become weaker as the load decreases, and it is gradually impossible to obtain the defect information from the vibration signals collected at point #1.

Figure 11 shows the acceleration signals in the X-direction at point #8 and point #0, respectively. It can be seen from Figure 11 that the vibration signals at point #8 are also affected by the load. When the load is large, the defect information can be clearly identified in the vibration signals of point #8. With the decrease of the load, the fault

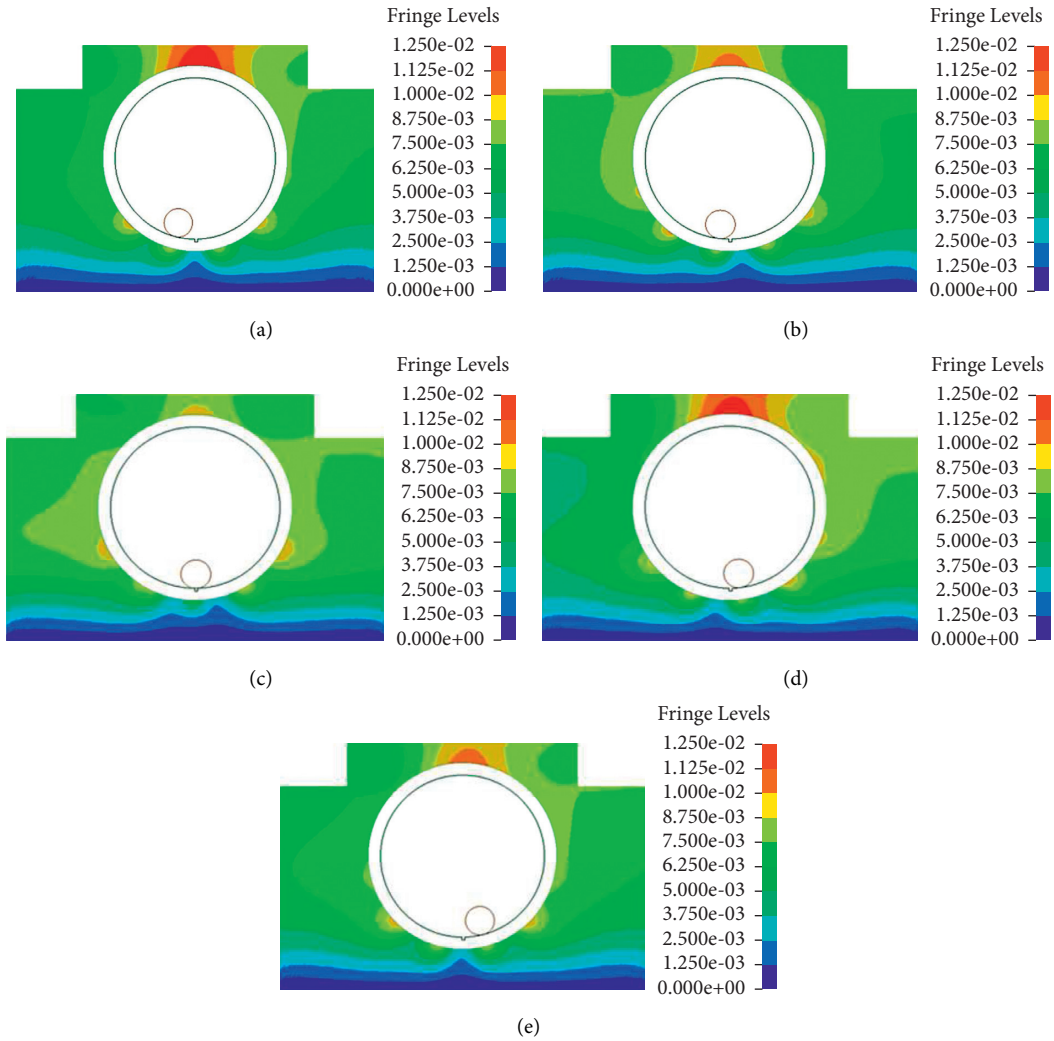

Figure 8: The deformation cloud diagram of the bearing housing while a rolling element is passing through the defect at different time instants: (a) 0.0697 s, (b) 0.0712 s, (c) 0.0727 s, (d) 0.0742 s, and (e) 0.0757 s.

characteristics are getting weaker. However, by comparing Figures 10(a) and 11(a), it is noted that the impact component in the vibration signal at point #8 under 2000 N load is more obvious than that at point #1.

In summary, as the load decreases, the defect characteristics contained in the vibration signals collected at points #1 and #8 become weaker. But under the same load condition, the vibration signal at point #8 is clearer than that at point #1. This is because the structural vibration of the bearing housing is greatly affected by the load, and the attenuation of vibration signal transmission is relatively less. Therefore, under the condition of light load, the sensor should be arranged at the position closest to the fault.

3.4. Analysis of Vibration Signals at Test Points under Different Speeds. The vibration signals in the Y-direction at measuring point #1 and the defect point #0 under rotational speeds of 2800 rpm, 2100 rpm, 1400 rpm, and 700 rpm are shown in Figure 12.

It can be seen from Figure 12 that the impact impulses due to the defect excitation are more obvious with the increase of speed. This is because the shorter the time interval between two adjacent rolling elements passing through the fault, the less the time required for the attenuation of impact vibration. As the speed decreases, the amplitudes of the vibration signals at points #0 and #1 decrease. The defect characteristics in the vibration signal are much more obvious at a speed of 1400 rpm. With the increase of the rotational speed, the vibration energy increases with the gradual appearance of noise. The impact components generated by the defect are gradually masked, and the defect characteristics in the vibration signals at point #1 become weaker. As the speed decreases, the vibration energy of the bearing decreases. The impact of the fault becomes slight, and the defect characteristics captured by the vibration signals at point #1 are limited.

Figure 13 shows the acceleration signals in the X-direction at point #8 and point #0, respectively. It can be seen from Figure 13 that when the speed is large, the vibration signals at

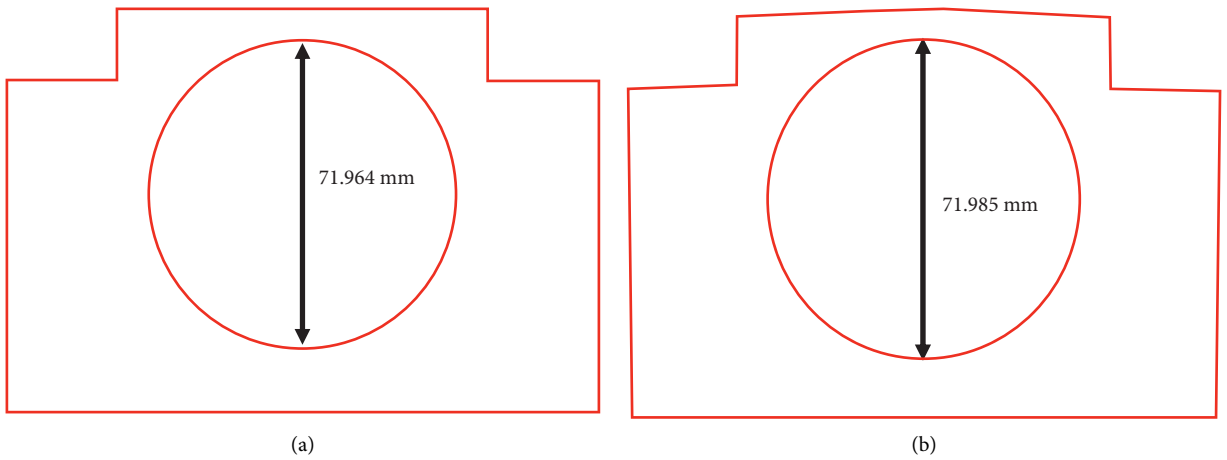

Figure 9: Deformation of bearing housing: (a) without deformation and (b) with deformation based on Figure 8(c) (note that the enlarged scale is 200).

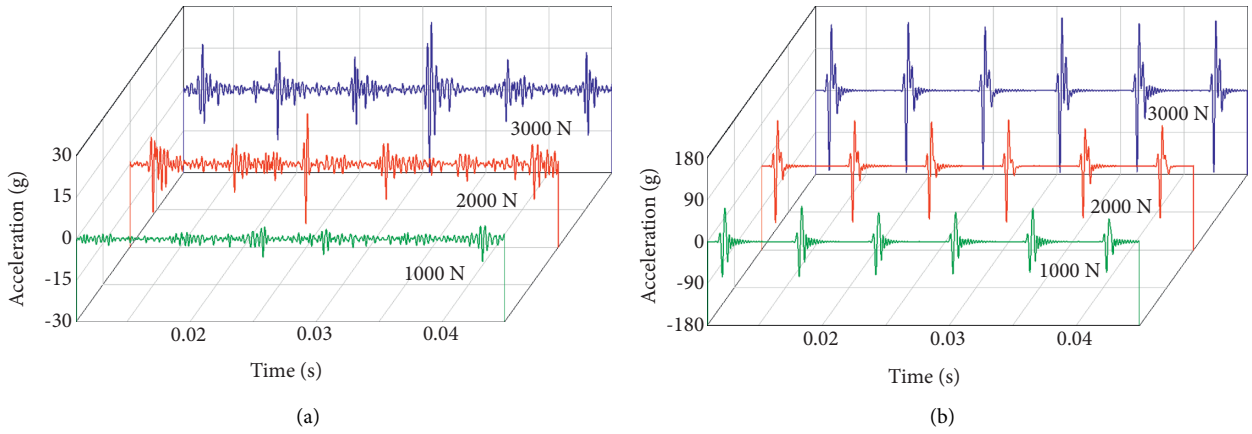

Figure 10: Acceleration signals under different loads at different points: (a) the measurement point #1 and (b) the defect point # 0.

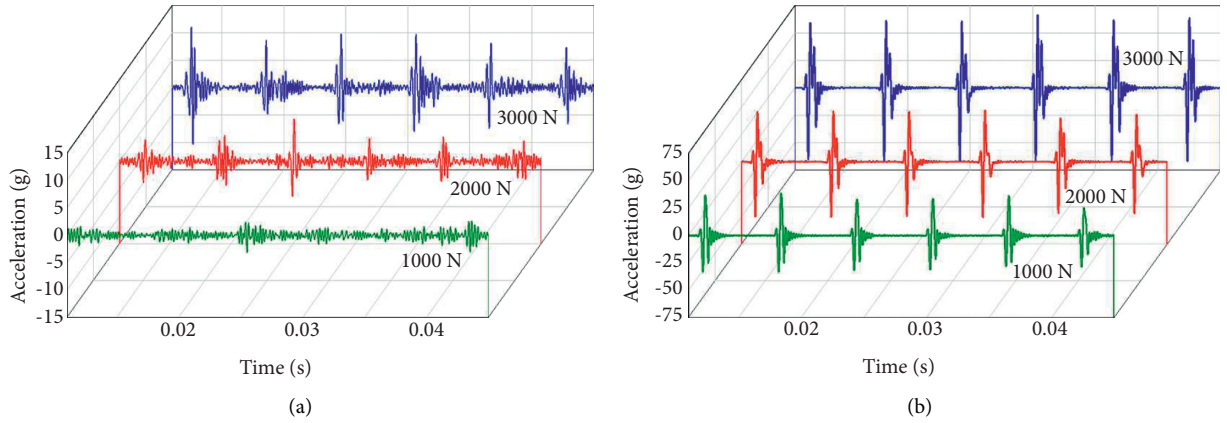

Figure 11: Acceleration signals under different loads at different points: (a) the measurement point #8 and (b) the defect point #0.

point #8 can clearly reflect the defect information. When the speed is small, the vibration signals at point #8 are greatly affected by the speed. When it decreases to a certain degree, it is almost impossible to obtain the defect information from the vibration signals at point #8. Comparing Figure 12(a) with Figure 13(a), it can be seen that when the rotation speed is large, the impact component in the vibration signal at point #8 is more obvious than that at point #1. When the rotation speed

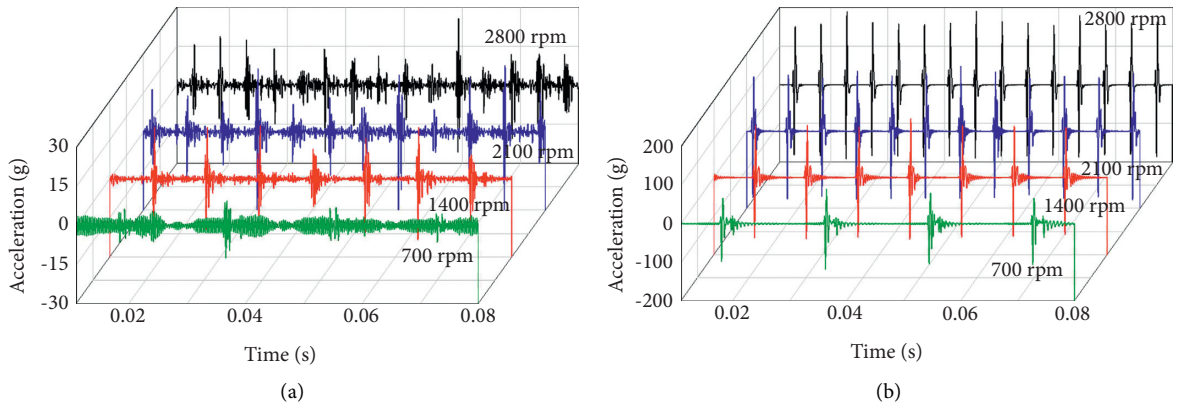

Figure 12: Acceleration signals under different speeds at different points: (a) the measurement point #1 and (b) the defect point #0.

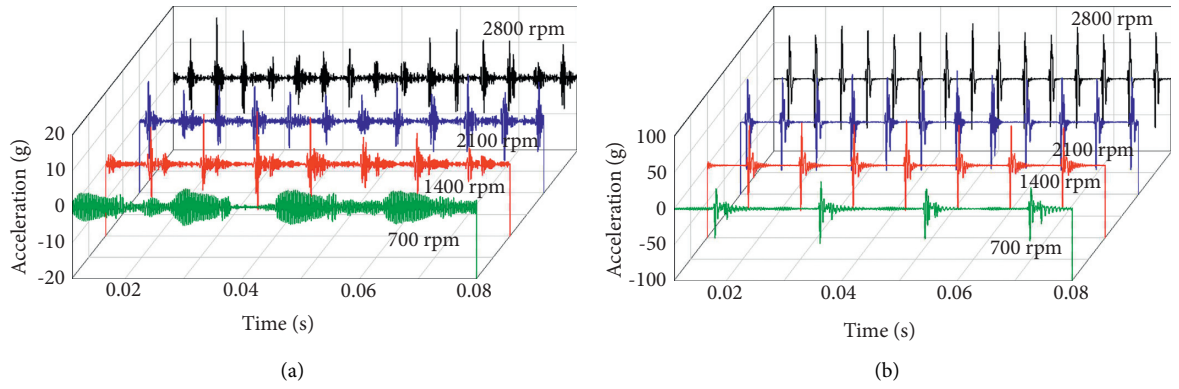

Figure 13: Acceleration signals under different speeds at different points: (a) the measurement point #8 and (b) the defect point #0.

is small, the impact component in the vibration signal at point # 1 is more obvious than that at point #8.

In summary, under the same high-speed working condition, the vibration signal at point #8 is better than that at point #1. Under the same low-speed working condition, the vibration signal at point #1 is better than that at point #8. This indicates that when the rotation speed is high, the influence of the rotation speed on the transmission of defect excitation is smaller than the structural vibration of the bearing housing. On the contrary, when the rotation speed is low, the influence of the rotation speed on the structural vibration of the bearing housing is less than the transmission of the defect excitation. Therefore, the sensor should be placed at the position closest to the fault under the condition of high speed and at the position where the structural stiffness is weakest under the condition of low speed.

4. Conclusion

In this article, a novel dynamic model of the rolling bearing-bearing system based on the elastic interface is established. Compared with previous finite element models, the proposed model uses sharing nodes and a contact pair between interfaces to simulate the interferences assembly relationship between the bearing and the housing. This allows the proposed model to faithfully reflect the contact conditions and simulate the attenuation phenomenon when the vibration signal transmits from the interior defect excitation point to the exterior measuring point. An experiment was conducted to verify the proposed model by directly comparing the simulated vibration responses and measured responses at the top surface and side surface of the bearing housing. In addition, the vibration transmission characteristics of the bearing housing system are studied. The influences of load and speed on the vibration signals at various measuring points are analyzed. The conclusions of this study include the following:

(1) The proposed dynamic model using a contact pair between interfaces to simulate the contact condition between the outer ring and the housing can provide a more accurate reflection on the contact interface stiffness and signal attenuation. These enable the proposed model to yield more consistent vibration results with experimentally measured results.

(2) The vibration distribution on the bearing housing surface is related to the bearing housing structure and the fault location. By studying the vibration transmission characteristics of the bearing-bearing housing system, it is found that the optimal measuring points on the outer surface of the bearing housing should be located at the position where the rigidity of the bearing housing structure is weak or the location is closest to the fault.

(3) Under the light load and high speed, the sensor should be placed at the location closest to the fault. However, under the low speed, the sensor should be placed in the position where the rigidity of the bearing housing structure is weak. These findings provide guidance for the sensor arrangement and improvement of fault diagnosis accuracy under different operating conditions.

Abbreviations

Symbols

C_b: The speed of bending waves
D_r: The bearing roller diameter
D_j ($j = i, o, m$): The bearing innter diameter ($j = i$), outer diameter ($j = o$), and pitch diameter ($j = m$)
E_i ($i = 1, 2$): The modulus of elasticity of bearing rolling element and races ($i = 1$) and cage ($i = 2$)
E_b: The bulk modulus in Figure 3
F_c: The normal contact force in Figure 3
g_n: The gap parameter in Figure 3
S_b: The area of elements in contact in equation (4)
T: The thickness of the bearing outer race
x^k ($k = 1, 2$): The positions of the two contact points in Figure 3
Z: The number of bearing rolling elements
α: The bearing contact angle
α_f: The scaling coefficient in equation (4)
ρ_i ($i = 1, 2$): The density of bearing rolling element and races ($i = 1$) and cage ($i = 2$)
v_i ($i = 1, 2$): Poisson's ratio of bearing rolling element and races ($i = 1$) and cage ($i = 2$)
ω: The angular frequency
λ: The distance parameter in equation (2)
ε_1: The radial clearance between roller and races
ε_2: The cage pocket clearance.

Data Availability

Data are available upon request through contacting the corresponding author (wennian.yu@cqu.edu.cn).

Conflicts of Interest

The authors declare that there are no conflicts of interest with respect to the research, authorship, and/or publication of this article.

Acknowledgments

The research work described in the article was supported by the National Natural Science Foundation of China (Project nos. 51965018, 51865010, and 5210050795).

References

[1] Y. Yang, C. Liu, and D. Jiang, "Vibration propagation identification of rotor-bearing-casing system using spatio-temporal graphical modeling," *Mechanism and Machine Theory*, vol. 134, pp. 24–38, 2019.

[2] R.-B. Sun, Z.-B. Yang, Z. Zhai, and X.-F. Chen, "Sparse representation based on parametric impulsive dictionary design for bearing fault diagnosis," *Mechanical Systems and Signal Processing*, vol. 122, pp. 737–753, 2019.

[3] J. Liu, Y. Xu, and G. Pan, "A combined acoustic and dynamic model of a defective ball bearing," *Journal of Sound and Vibration*, vol. 501, Article ID 116029, 2021.

[4] W. Tu, J. Yang, W. Yu, and Y. Luo, "Contact characteristic and vibration mechanism of rolling element bearing in the process of fault evolution," *Proceedings of the Institution of Mechanical Engineers - Part K: Journal of Multi-Body Dynamics*, vol. 235, no. 1, pp. 19–36, 2021.

[5] A. Chen and T. R. Kurfess, "Signal processing techniques for rolling element bearing spall size estimation," *Mechanical Systems and Signal Processing*, vol. 117, pp. 16–32, 2019.

[6] S. Singh, U. G. Köpke, C. Q. Howard, and D. Petersen, "Analyses of contact forces and vibration response for a defective rolling element bearing using an explicit dynamics finite element model," *Journal of Sound and Vibration*, vol. 333, no. 21, pp. 5356–5377, 2014.

[7] S. Singh, C. Q. Howard, C. H. Hansen, and U. G. Köpke, "Analytical validation of an explicit finite element model of a rolling element bearing with a localised line spall," *Journal of Sound and Vibration*, vol. 416, pp. 94–110, 2018.

[8] A. Moazen Ahmadi, D. Petersen, and C. Howard, "A non-linear dynamic vibration model of defective bearings - the importance of modelling the finite size of rolling elements," *Mechanical Systems and Signal Processing*, vol. 52-53, pp. 309–326, 2015.

[9] U. K. A. Patel and S. H. Upadhyay, "Nonlinear dynamic response of cylindrical roller bearing-rotor system with 9 degree of freedom model having a combined localized defect at inner-outer races of bearing," *Tribology Transactions*, vol. 60, no. 2, pp. 284–299, 2017.

[10] Z. Shi, J. Liu, H. Li, Q. Zhange, and G. Xiao, "Dynamic simulation of a planet roller bearing considering the cage bridge crack," *Engineering Failure Analysis*, vol. 131, Article ID 105849, 2021.

[11] J. Liu, C. Tang, and G. Pan, "Dynamic modeling and simulation of a flexible-rotor ball bearing system," *Journal of Vibration and Control*, 2021.

[12] Y. M. Shao, Z. G. Chen, X. J. Zhou, and L. Ge, "Study on decaying of shock vibration energy during transmission through multi-interfaces in gear-shaft-bearing-housing system," *Zhendong yu Chongji/Journal Vib Shock*, vol. 6, 2009.

[13] H. Alian, S. Konforty, U. Ben-Simon, R. Klein, M. Tur, and J. Bortman, "Bearing fault detection and fault size estimation using fiber-optic sensors," *Mechanical Systems and Signal Processing*, vol. 120, pp. 392–407, 2019.

[14] M. F. While, "Rolling element bearing vibration transfer characteristics: effect of stiffness," *Journal of Applied Mechanics*, vol. 46, no. 3, pp. 677–684, 1979.

[15] T. C. Lim and R. Singh, "Vibration transmission through rolling element bearings, part I: bearing stiffness formulation," *Journal of Sound and Vibration*, vol. 139, no. 2, pp. 179–199, 1990.

[16] Y. Gao, Z. Li, J. Wang, X. Li, and Q. An, "Influences of bearing housing deflection on vibration performance of cylinder roller bearing-rotor system," *Proceedings of the Institution of Mechanical Engineers - Part K: Journal of Multi-Body Dynamics*, vol. 227, no. 2, pp. 106–114, 2013.

[17] J. Kraus, J. J. Blech, and S. G. Braun, "In situ determination of rolling bearing stiffness and damping by modal analysis," *Journal of Vibration and Acoustics*, vol. 109, no. 3, pp. 235–240, 1987.

[18] D. P. Fleming, *Vibration Transmission through Bearings with Application to Gearboxes*, National Aeronautics and Space Administration Glenn Research Center, Cleveland, OH, USA, 1987.

[19] J. Liu, Y. Shao, and T. C. Lim, "Impulse vibration transmissibility characteristics in the presence of localized surface defects in deep groove ball bearing systems," *Proceedings of the Institution of Mechanical Engineers - Part K: Journal of Multi-Body Dynamics*, vol. 228, no. 1, pp. 62–81, 2014.

[20] J. Liu, Y. Xu, and Y. Shao, "Dynamic modelling of a rotor-bearing-housing system including a localized fault," *Proceedings of the Institution of Mechanical Engineers - Part K: Journal of Multi-Body Dynamics*, vol. 232, no. 3, pp. 385–397, 2018.

[21] J. Liu, C. Tang, and Y. Shao, "An innovative dynamic model for vibration analysis of a flexible roller bearing," *Mechanism and Machine Theory*, vol. 135, pp. 27–39, 2019.

[22] H. Xiao, X. Zhou, J. Liu, and Y. Shao, "Vibration transmission and energy dissipation through the gear-shaft-bearing-housing system subjected to impulse force on gear," *Measurement*, vol. 102, pp. 64–79, 2017.

[23] G. Chen and M. Qu, "Modeling and analysis of fit clearance between rolling bearing outer ring and housing," *Journal of Sound and Vibration*, vol. 438, pp. 419–440, 2019.

[24] B. Wang, J.-y. Zhang, L.-x. Gao, Y.-G. Xu, and L.-L. Cui, "Dynamic response analysis for rolling bearing vibration measuring point," *Journal of Vibration and Shock*, vol. 31, no. 19, pp. 166–168, 2012.

[25] Z. Cao, Y. Chen, and L. Zang, "Model-based transmission acoustic analysis and improvement," *Proceedings of the Institution of Mechanical Engineers - Part D: Journal of Automobile Engineering*, vol. 234, no. 6, pp. 1572–1584, 2020.

[26] C. Xiang, C. Song, C. Zhu, Y. Weng, and W. Guo, "Effects of tooth modifications on the mesh and dynamic characteristics of differential gearbox used in electric vehicle," *Iranian Journal of Science and Technology, Transactions of Mechanical Engineering*, vol. 43, no. S1, pp. 537–549, 2019.

[27] J. Liu, Y. Xu, Y. Shao, H. Xiao, and H. Li, "The effect of a localized fault in the planet bearing on vibrations of a planetary gear set," *The Journal of Strain Analysis for Engineering Design*, vol. 53, no. 5, pp. 313–323, 2018.

[28] X. Yu, Y. Sun, D. Zhao, and S. Wu, "A revised contact stiffness model of rough curved surfaces based on the length scale," *Tribology International*, vol. 164, Article ID 107206, 2021.